Entropy Generation and Thermal Analysis on MHD Second-Grade Fluid with Variable Thermophysical Properties over a Stratified Permeable Surface of Paraboloid Revolution

Meshal Shutaywi, Muhammad Rooman, Muhammad Asif Jan, Narcisa Vrinceanu,* Zahir Shah,* and Wejdan Deebani

ACCESS | Metrics & More | Article Recommendations

ABSTRACT: Stratification is used in a wide range of energy storage fields, including solar thermal energy systems. This paper investigates entropy optimization and the effects of heat production, magnetic field, and various fluid parameters on the flow of second-grade fluid through unstratified and stably stratified paraboloids of revolution. In the heat transfer equation, stratification, linear thermal radiation, and Joule dissipation have all been explored. The similarity transformation is used to convert the governing PDEs into nonlinear ODEs. The HAM (homotopy analysis method) is used to solve dimensionless nonlinear ODEs. The impact of significant elements on various profiles is exposed and explored. Graphical results are used to examine the influence of the velocity profile, temperature, concentration, and entropy formation rate using tables to indicate the characteristics of skin friction, Nusselt number, and Sherwood number for numerous parameters. It is noticed that the velocity is enhanced by raising the stratification parameter, while the opposite behavior is observed for temperature distribution. The concentration profile declined as the solute stratification parameter was enhanced. For both the unstratified and stratified regions, incremental values of the Brinkman number and magnetic parameter depict augmentation in entropy production, while entropy production drops for a large value of the temperature ratio parameter.
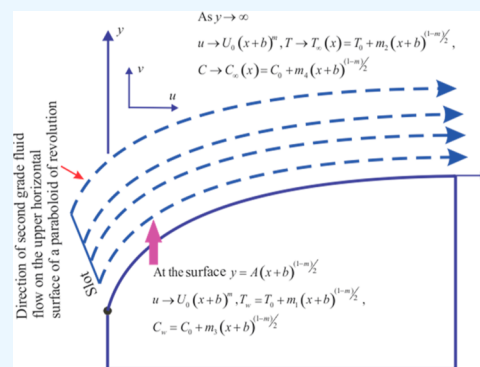
1. INTRODUCTION

The dynamics of today's world have been altered by two sorts of fluids: Newtonian and non-Newtonian fluids. Researchers first focused on Newtonian fluids, but due to the complexity and variety of numerous fluid-dependent procedures, the importance of non-Newtonian fluids is growing. Non-Newtonian fluids are important for a variety of economic, physiological, physical, industrial, medical, mechanical, and technical applications. Therefore, the narrative of non-Newtonian fluids is necessary for a better understanding of such phenomena. It can be executed by contrasting Newtonian and non-Newtonian flow behavior. One significant distinction between these two fundamental kinds of fluids is that Newtonian fluids have a linear association between shear stress and strain rates, but non-Newtonian fluids do not. Non-Newtonian fluids exhibit complex properties as a result of this relationship and are classified into subdivisions such as shear thickening, shear-thinning, thixotropic, and dilatant fluids. Rheologists have discovered that several fluid models, such as second-grade fluid, which explains the properties of shear thickening, shear-thinning, and Newtonian fluid, behave differently under different conditions. Second-grade fluid is famous and valuable among investigators because of its dynamic characteristics. Vajravelu and Roper[1]

conducted thermal and dynamical investigations of second-grade fluids. The perturbation technique was used by Rajeswari and Rathna[2] to explore the dynamics of the stagnant second-grade fluid. Rajeswari and Rathna[2] were followed by Grag and Rajagopal,[3] who found complete consensus with their outcomes. Fetecau and Fetecau[4] used the Hankel transform approach to provide a solution for second-grade fluids caused by using an oscillating circular cylinder. Recently, Abbas et al.[5] scrutinize the stagnation point flow of viscoelastic second-grade fluid across a stretching cylinder in the presence of the thermal slip and MHD effects.

Many scientists have looked into fluid flow on a variety of surfaces, including inclined, horizontal, and vertical surfaces. A revolutionary paraboloid is an object with a changeable thickness on the top half face. Davis and Werle[6] developed a

new method for resolving the laminar flow across a revolutionary paraboloid in 1972. According to Makinde and Animasaun et al.,[7] fluid flows over surfaces of different thicknesses or non-uniform thicknesses are described as the topmost horizontal surface of a revolutionary paraboloid. Fluid flows over a revolutionary paraboloid have piqued scientists' interest due to the numerous applications of flows over a variable thickness surface. Zeeshan et al.[8] considered the flow of a Casson fluid containing nanoparticles across a horizontal revolution surface. Magnetite possessed a three-dimensional structure. Abdeljawad et al.[9] clarified Carreau fluid flow on a horizontal revolutionary paraboloid surface with a thermal radiation effect. The Catteneo-Christov model was used by Kalyani et al.[10] in a micropolar fluid with varying thickness.

The stacking of bodies of water as a result of temperature and concentration changes is known as stratification. The stratification idea is used to retain cold and warm water in the same tank and separate the two distinct masses of water using a thin layer thermocline in various energy storage applications like thermal storage systems or solar thermal utilization systems. Khan et al.[11] recently discussed the impact of temperature and solutal stratification on the chemically reactive flow of the hyperbolic tangent fluid. In a stratified medium, Dawar et al.[12] explored the bioconvection flow of a binary fluid comprising nanoparticles and gyrotactic bacteria. Khan et al.[13] demonstrated the effect of stratification on the nonlinear radiative flow of nanoparticles. The influence of the stratification parameter and Atwood number on the compressible multi-mode Rayleigh−Taylor uncertainty was investigated by Luo and Wang.[14] The dynamics of the buoyant convective flow of a micropolar fluid under temperature stratification were studied by Koriko et al.[15] The existence of stratification was shown to be associated with a decrease in fluid velocity and temperature. Pattnaik et al.[16] investigated the flow of electrically conducting micropolar nanofluids from a vertical stretching surface adjacent to a porous medium in the presence of a transverse magnetic field. They took into account both thermal and solutal stratifications, as well as chemical reaction effects, viscous dissipation, and heat sources.

Entropy optimization is the quantity of entropy produced by irreversible processes such as fluid flow over thermal radiation, heat flow over a thermal resistance, Joule heating, diffusion, fluid viscosity inside a system, friction between solid surfaces, and so on in a thermodynamic system. During a reversible process, the entire entropy of the system remains unaltered, according to the second rule of thermodynamics. It is commonly understood that entropy creation plays a critical role in reducing the system's required energy sources. The researchers' main concern in order to enhance effectiveness and achievement in most industrial and engineering applications is to reduce entropy formation. With this in mind, Bejan[17] attempted to examine entropy formation in a convective heat transmission process at first. Shit et al.[18] explored entropy formation in unstable two-dimensional MHD nanoparticles flowing through an exponentially extending surface in a porous medium under the effect of thermal radiation using a mathematical model. Shit and Mandal[19] expanded on this research. They utilized Buongiorno's model to look into the creation of entropy in an unstable MHD flow of Casson nanoparticles through a stretching vertical plate under the effect of thermal radiation. Bhatti et al.[20] investigated the production of entropy during the interaction of nanomaterials with a stretching permeable sheet and nonlinear thermal radiation. Kumar et al.[21] investigated the 2D stagnation point hydro-

magnetic flow of Casson nanoparticles across a stretching surface in a non-Darcy permeable medium to Arrhenius activation energy-stimulated binary chemical reaction. Bhatti et al.[22] go into great detail about the behavior of diamond (C) and silica (SiO_2) nanoparticles dissolved in a water-based hybrid nanofluid lying above an exponentially elastic surface. They assumed the porous medium when analyzing the flow behavior. Bhatti et al.[23] discuss the development of a mathematical model of hybrid magnesium oxide (MgO) and nickel (Ni) nanofluid MHD stagnation point flow impinging on a permeable elastic stretching surface in a permeable medium. Zhang et al.[24] explored the role of the induced magnetic effect on hybrid nanofluid flow via a stretchy surface. Kristiawan et al.[25] evaluated and deduced that the existence of TiO_2/water nanofluids in different volumetric concentrations improved the heat transfer coefficient of microfins. A considerable amount of notable work has recently been accomplished.[26−30]

The main goal of this article is to examine the entropy optimization and the effect of variable fluid features on the flow of the second-grade fluid across a surface that is neither inclined nor vertical but rather has a non-uniform thickness. Several factors, including Joule dissipation, heat radiation, stratification, and variable thermal conductivity, have been used to model the energy equation. The flow problem equations are presented and transformed using a suitable similarity transformation. The arising equations are solved using HAM. A concise graphical explanation is provided in a separate section, and the conclusion of relevant material restrictions is accurately depicted. As far as we know, no one has addressed this issue.

2. MATHEMATICAL FORMULATION

Consider a steady, MHD, incompressible second-grade fluid flow along the horizontal surface of a paraboloid of revolution, with varying fluid characteristics and stratifications. The domain $A(x + b)^{1-m/2} \leq y < \infty$ where $A \geq 0$ is supposed to be occupied by the second-grade fluid flow across the surface with non-uniform thickness. m is the velocity index, and A and b are arbitrary constants related to the thickness of the surface. m is less than 1 in this study. The fluid layers on an upper horizontal revolution surface are stretched at $U_w = U_0(x + b)^m$, where U_0 is the reference velocity. It is assumed that the horizontal surface of the revolutionary paraboloid is porous. The −axis , on the other hand, represents the stretchy surface's orientation, while the $y -$ axis is perpendicular to it.

Under the impact of variable fluid characteristics and stratifications, the equations regulating the dynamics of the second-grade fluid over the upper horizontal surface of the paraboloid of revolution are written as

$$\frac{\partial u}{\partial x} + \frac{\partial v}{\partial y} = 0 \tag{1}$$

$$u\frac{\partial u}{\partial x} + v\frac{\partial u}{\partial y} = \frac{1}{\rho}\frac{\partial}{\partial y}\left(\mu(T)\frac{\partial u}{\partial y}\right) + \frac{\alpha_1}{\rho}\left(\frac{\partial u}{\partial x}\frac{\partial^2 u}{\partial y^2} + u\frac{\partial^3 u}{\partial x \partial y^2}\right. $$
$$\left. - \frac{\partial u}{\partial y}\frac{\partial^2 u}{\partial x \partial y} + v\frac{\partial^3 u}{\partial y^3}\right) - \frac{\sigma B_0^2}{\rho}u - \frac{\mu(T)}{\rho k_1}u \tag{2}$$

$$u\frac{\partial T}{\partial x} + v\frac{\partial T}{\partial y} = \frac{1}{\rho c_p}\frac{\partial}{\partial y}\left(k(T)\frac{\partial T}{\partial y}\right) + \frac{1}{\rho c_p}\left(\frac{16\sigma^* T_0^3}{3k^*}\right)\frac{\partial^2 T}{\partial y^2}$$

$$+ \frac{\sigma B_0^2}{\rho c_p}u^2 + \frac{Q_0(T_w - T_0)}{\rho c_p}$$

$$e^{-n\sqrt{\frac{U_0(m+1)}{2\vartheta}}(x+b)^{m-1/2}} \tag{3}$$

$$u\frac{\partial C}{\partial x} + v\frac{\partial C}{\partial y} = D\frac{\partial^2 C}{\partial y^2} - K^*(C - C_\infty) \tag{4}$$

Subjected to boundary conditions

$$u = U_0(x+b)^m, \; v = 0,$$

$$T = T_w, \; C = C_w \; at \; y = A(x+b)^{1-m/2}$$

$$u \to 0, \; T \to T_\infty, \; C \to C_\infty \quad at \quad y \to \infty \tag{5}$$

Batchelor's[31] experimental results were used to develop a temperature-dependent viscosity mathematical model, along with the temperature-dependent thermal conductivity mathematical model of Charraudeau[30] as

$$\mu(T) = \mu_\infty[1 + b(T_w - T)]$$

$$k(T) = k_\infty[1 + \delta(T - T_\infty)] \tag{6}$$

As we describe the thermal stratification at the wall T_w and solutal stratification at the wall C_w, as well as the free stream temperature and concentration (T_∞ and C_∞), it is critical to show how stratification is included into the energy and concentration equations.

$$T_w = T_0 + m_1(x+b)^{1-m/2}$$

$$T_\infty = T_0 + m_2(x+b)^{1-m/2} \tag{7}$$

$$C_w = C_0 + m_3(x+b)^{1-m/2}$$

$$C_\infty = C_0 + m_4(x+b)^{1-m/2} \tag{8}$$

where T_0 represents the reference temperature; it is worthy to note that stratification happens for all places of x on the wall at $y = A(x+b)^{1-m/2}$, as well as for all points of x at the ambient temperature as $y \to \infty$.

The similarity variable η and the stream function $\psi(x, y)$ can be expressed as

$$u = \frac{\partial \psi}{\partial y}, \; v = -\frac{\partial \psi}{\partial x} \tag{9}$$

$$\eta = y\sqrt{\frac{U_0(m+1)}{2\vartheta}}(x+b)^{m-1/2},$$

$$\psi = \sqrt{\frac{2\vartheta U_0}{m+1}}(x+b)^{m+1/2}f(\eta)$$

$$\theta(\eta) = \frac{T - T_\infty}{T_w - T_0}, \; \phi(\eta) = \frac{C - C_\infty}{C_w - C_0} \tag{10}$$

The governing partial differential eqs 2−4, as well as the boundary constraints 5 are changed to a system of nonlinear differential equations represented as a stream function $\psi(x, y)$

that satisfies the continuity equation via similarity transformation.

$$[1 + (1 - S_t - \theta)\xi]\frac{d^3 f}{d\eta^3} - \xi\frac{d\theta}{d\eta}\frac{d^2 f}{d\eta^2}$$

$$+ \lambda_1\left[\begin{array}{c}(3m-1)\frac{df}{d\eta}\frac{d^3 f}{d\eta^3} - \frac{3m-1}{2}\frac{d^2 f}{d\eta^2}\frac{d^2 f}{d\eta^2} \\ -\frac{m+1}{2}f\frac{d^4 f}{d\eta^4}\end{array}\right]$$

$$-\frac{2m}{m+1}\frac{df}{d\eta}\frac{df}{d\eta} + f\frac{d^2 f}{d\eta^2} - \frac{2}{m+1}M\frac{df}{d\eta}$$

$$-\frac{2}{m+1}\beta[1 + (1 - S_t - \theta)\xi]\frac{df}{d\eta} = 0 \tag{11}$$

$$[(1 - \varepsilon\theta) + Rd]\frac{d^2 \theta}{d\eta^2} + \varepsilon\frac{d\theta}{d\eta}\frac{d\theta}{d\eta}$$

$$+ \frac{2}{m+1}Pr\,\gamma e^{-n\eta} + \frac{2}{m+1}MPrEc\frac{df}{d\eta}\frac{df}{d\eta}$$

$$- Pr\left(\frac{1-m}{1+m}S_t\frac{df}{d\eta} + \frac{1-m}{1+m}\theta\frac{df}{d\eta} - f\frac{d\theta}{d\eta}\right) = 0 \tag{12}$$

$$\frac{d^2 \phi}{d\eta^2} - \frac{2}{m+1}S_c\zeta\phi - S_c\left(\frac{1-m}{1+m}S_0\frac{df}{d\eta} + \frac{1-m}{1+m}S_0\phi\frac{df}{d\eta}\right.$$

$$\left. - f\frac{d\phi}{d\eta}\right) = 0 \tag{13}$$

It is worth noting that $y = A(x+b)^{1-m/2}$; the slightest value of y that corresponds to the slightest value of the similarity variable is found at the surface

$$\eta = A\sqrt{\frac{U_0(m+1)}{2\vartheta}} = F \tag{14}$$

Therefore, the boundary constraints become

$$f(F) = F\frac{1-m}{1+m}, \; \frac{df}{fF} = 1, \; \theta(F) = 1 - S_t$$

$$, \phi(F) = 1 - S_0 \; at \; F = \eta$$

$$\frac{df}{dF} \to 0, \; \theta(F) \to 0,$$

$$\phi(F) \to 0 \; as \quad F \to \infty \tag{15}$$

The boundary conditions are dependent on F, while the modified governing eqs 11−13 are dependent on η. It is imperative to change the domain from $[F, \infty]$ to $[0, \infty]$ which is carried out by defining $F(\chi) = F(\eta - \chi) = f(\eta), \; \Theta_1(\chi) = \Theta_1(\eta - F) = \theta(\eta)$ and $\varphi(\chi) = \varphi(\eta - F) = \phi(\eta)$. The non-dimensional governing eqs 11−13 are rewritten as

$$[1 + (1 - S_t - \Theta_1)\xi]\frac{d^3F}{d\chi^3} - \xi\frac{d\theta_1}{d\chi}\frac{d^2F}{d\chi^2}$$

$$+ \lambda_1\left[\begin{array}{c}(3m - 1)\dfrac{dF}{d\chi}\dfrac{d^3F}{d\chi^3} - \dfrac{3m - 1}{2}\dfrac{d^2F}{d\chi^2}\dfrac{d^2F}{d\chi^2} \\ - \dfrac{m + 1}{2}F\dfrac{d^4F}{d\chi^4}\end{array}\right]$$

$$- \frac{2m}{m + 1}\frac{dF}{d\chi}\frac{dF}{d\chi} + F\frac{d^2F}{d\chi^2} - \frac{2}{m + 1}M\frac{dF}{d\chi}$$

$$- \frac{2}{m + 1}\beta[1 + (1 - S_t - \theta_1)\xi]\frac{dF}{d\chi} = 0 \tag{16}$$

$$[(1 - \varepsilon\Theta_1) + Rd]\frac{d^2\Theta_1}{d\chi^2} + \varepsilon\frac{d\Theta_1}{d\chi}\frac{d\Theta_1}{d\chi}$$

$$+ \frac{2}{m + 1}Pr\,\gamma e^{-n\chi} + \frac{2}{m + 1}MPrEc\frac{dF}{d\chi}\frac{dF}{d\chi} -$$

$$Pr\left(\frac{1 - m}{1 + m}S_t\frac{dF}{d\chi} + \frac{1 - m}{1 + m}\Theta_1\frac{dF}{d\chi} - F\frac{d\Theta_1}{d\chi}\right) = 0 \tag{17}$$

$$\frac{d^2\varphi}{d\chi^2} - \frac{2}{m + 1}Sc\zeta\varphi - Sc\left(\frac{1 - m}{1 + m}S_0\frac{dF}{d\chi} + \frac{1 - m}{1 + m}S_0\varphi\frac{dF}{d\chi}\right.$$

$$\left. - F\frac{d\varphi}{d\chi}\right) = 0 \tag{18}$$

The boundary constraints become

$$f(\chi) = F\frac{1 - m}{1 + m},\ \frac{dF}{d\chi} = 1,$$

$$\Theta_1(\chi) = 1 - S_t,$$

$$\varphi(\chi) = 1 - S_0 \text{ at } \chi = 0$$

$$\frac{dF}{d\chi} \to 0,\ \Theta_1(\chi) \to 0,$$

$$\varphi(\chi) \to 0 \text{ as } \chi \to \infty \tag{19}$$

where

$$\xi = bm_1x,\ M = \frac{\sigma B_0^2}{\rho U_0}(x + b)^{1-m},$$

$$\beta = \frac{\mu}{\rho k_1 U_0}(x + b)^{1-m},\ S_t = \frac{m_2}{m_1},$$

$$\lambda_1 = \frac{\alpha_1 U_0}{\rho\vartheta}(x + b)^{m-1},\ Pr = \frac{\vartheta\rho c_p}{k_\infty},$$

$$Ec = \frac{U_0^2}{c_p m_1}(x + b)^{5m-1},$$

$$Rd = \frac{4\sigma^* T_\infty^3}{k^* k_\infty},\ \gamma = \frac{Q_0}{\rho c_p(x + b)^{m-1}}$$

$$\zeta = \frac{K^*}{U_0(x + b)^{m-1}},\ \varepsilon = \delta m_1 x,$$

$$Sc = \frac{\vartheta}{D},\ S_0 = \frac{m_4}{m_3},\ Br = Ec.\,Pr \tag{20}$$

The following are the definitions of the skin friction, the local Nusselt number, and the Sherwood number

$$C_f = \frac{\tau_\omega}{\rho U_\omega^2},\ N_u = \frac{q_\omega}{k_\infty(T_w - T_0)},$$

$$S_h = \frac{q_m}{D(C_w - C_0)} \tag{21}$$

where τ_ω and q_ω are the surface shear stress and heat flux, respectively. These are defined as

$$\tau_\omega = \left[\mu(T)\left(\frac{\partial u}{\partial y}\right) + \alpha_1\left(\begin{array}{c}2\dfrac{\partial u}{\partial x}\dfrac{\partial u}{\partial y} + \\ u\dfrac{\partial^2 u}{\partial x\partial y} + v\dfrac{\partial^2 u}{\partial y^2}\end{array}\right)\right]_{y=A(x+b)^{1-m/2}}$$

$$q_\omega = -\left(k(T) + \frac{16\sigma^* T_\infty^3}{3k^*}\right)\left(\frac{\partial T}{\partial y}\right)_{y=A(x+b)^{1-m/2}}$$

$$q_m = -D\left(\frac{\partial C}{\partial y}\right)\Big|_{y=A(x+b)^{1-m/2}} \tag{22}$$

The dimensionless physical quantities are

$$Re_x^{1/2}C_f = \left[1 + \left(\begin{array}{c}1 - S_t \\ - \Theta_1(0)\end{array}\right)\xi\right]\frac{d^2F}{d\chi^2}(0) +$$

$$\lambda_1\left(\begin{array}{c}\dfrac{3m - 1}{2}\dfrac{d^2F}{d\chi^2}(0)\dfrac{d^2F}{d\chi^2}(0) - \\ \dfrac{m + 1}{2}F(0)\dfrac{d^3F}{d\chi^3}(0) + 2\dfrac{dF}{d\chi}(0)\dfrac{d^2F}{d\chi^2}(0)\end{array}\right) \tag{23}$$

$$Re_x^{-1/2} N_u = -[(1 - \varepsilon\Theta_1(0)) + Rd]\frac{d\Theta_1}{d\chi}(0) \qquad (24)$$

$$Re_x^{-1/2} S_h = -\frac{d\varphi}{d\chi}(0) \qquad (25)$$

3. ENTROPY OPTIMIZATION

Entropy optimization is the quantity of entropy produced by irreversible processes such as heat flow over a thermal resistance and Joule heating in thermodynamic system. Such as

$$S_g = \begin{array}{l} \dfrac{1}{T_0^2}\left(k(T) + \dfrac{16\sigma^* T_0^3}{3k^*}\right)\left(\dfrac{\partial T}{\partial y}\right)^2 + \\[12pt] \dfrac{\sigma B_0^2}{T_0}u^2 + \dfrac{\mu(T)}{T_0}\left(\dfrac{\partial u}{\partial y}\right)^2 + \\[12pt] \dfrac{\alpha_1}{T_0}\begin{pmatrix} u\dfrac{\partial u}{\partial y}\dfrac{\partial^2 u}{\partial x \partial y} + \dfrac{\partial u}{\partial x}\left(\dfrac{\partial u}{\partial y}\right)^2 \\[12pt] + v\dfrac{\partial u}{\partial y}\dfrac{\partial^2 u}{\partial y^2} + \dfrac{\partial v}{\partial y}\left(\dfrac{\partial u}{\partial y}\right)^2 \end{pmatrix} \end{array} \qquad (26)$$

Using transformations 9 and 10, the non-dimensional entropy formation is obtained as

$$\begin{aligned} N_g = {} & ((1 + \varepsilon\theta) + Rd)\theta'^2 + \frac{MBr}{\Omega}f'^2 \\ & + \frac{Br}{\Omega}\frac{m+1}{2}\left[1 + \left(\frac{1 - S_t}{-\Theta_1(0)}\right)\xi\right]f''^2 + \\ & \lambda_1\frac{Br}{\Omega}\frac{m+1}{2}\left(\frac{3m-1}{2}f'f''^2 - \frac{m+1}{2}ff''f'''\right) \end{aligned} \qquad (27)$$

Equation 27 is dependent on η. It is imperative to change the domain from $[F, \infty]$ to $[0, \infty]$ which is done by defining $F(\chi) = F(\eta - \chi) = f(\eta)$, $\Theta_1(\chi) = \Theta_1(\eta - F) = \theta(\eta)$, and $N_G(\chi) = N_G(\eta - F) = N_g(\eta)$.

$$N_G = \begin{array}{l} ((1 + \varepsilon\Theta_1) + Rd)\left(\dfrac{d\Theta_1}{d\chi}\right)^2 + \dfrac{MBr}{\Omega}\left(\dfrac{dF}{d\chi}\right)^2 \\[12pt] + \dfrac{Br}{\Omega}\dfrac{m+1}{2}\left[1 + \left(\dfrac{1 - S_t}{-\Theta_1(0)}\right)\xi\right]\left(\dfrac{d^2 F}{d\chi^2}\right)^2 \\[12pt] + \lambda_1\dfrac{Br}{\Omega}\dfrac{m+1}{2}\begin{pmatrix} \dfrac{3m-1}{2}\dfrac{dF}{d\chi}\left(\dfrac{d^2 F}{d\chi^2}\right)^2 \\[12pt] - \dfrac{m+1}{2}F\dfrac{d^2 F}{d\chi^2}\dfrac{d^3 F}{d\chi^3} \end{pmatrix} \end{array} \qquad (28)$$

Where $N_g = \frac{\vartheta T_0^2 S_g}{k U_0 (T_w - T_0)^2}(x + b)^{1-m}$ represents the total entropy formation, $\Omega = \frac{T_w - T_0}{T_0}$ represents the temperature ratio parameter, and $Re_x = \sqrt{\frac{2U_0(x+b)^{m+1}}{\vartheta(m+1)}}$ represents the local Reynolds number.

4. BEJAN NUMBER

The Bejan number (Be) is a number that demonstrates the value of thermal irreversibility in comparison to absolute irreversibility.

$$Be = \frac{((1 + \varepsilon\Theta_1) + Rd)\left(\frac{d\Theta_1}{d\chi}\right)^2}{N_G} \qquad (29)$$

5. RESULTS AND DISCUSSION

This section explains how to interpret the behavior of the various parameters on the profiles when they are set to fixed values. The plots in this study took into account the situations of $S_t = S_0 = 0$ (unstratified surface) and $S_t = S_0 = 1$ (stably stratified surface). Figures 1 and 2a,b show the outcome of
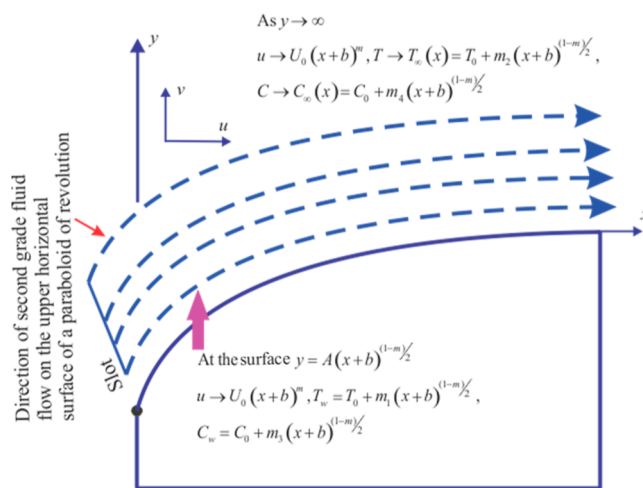

Figure 1. Physical sketch of the flow.

changing the velocity index m on the velocity field when $S_t = S_0 = 0$ and $S_t = S_0 = 1$. It can be seen in these images that there is no considerable rise in velocity fields as m is altered, although the profiles do slightly increase for bigger values of m. Figure 2c,d depicts the stimulus of the second-grade fluid parameter λ_1 on the velocity field for $S_t = S_0 = 0$ and $S_t = S_0 = 1$. The velocity field for both cases $S_t = S_0 = 0$ and $S_t = S_0 = 1$ is strengthened with increasing values of the second-grade fluid parameter, as seen in figures. This rise in the velocity field occurs because an increase in λ_1 causes a drop in fluid viscosity, which causes the velocity field in the flow zone to upsurge. In addition, as the second-grade fluid parameter grows, the boundary layer thickness of the momentum also rises. Figure 2e,f shows the outcome of the magnetic parameter M on the velocity field for $S_t = S_0 = 0$ and $S_t = S_0 = 1$. The figures show that at rising levels of the magnetic parameter in the flow zone, the velocity is eventually suppressed. This reduction in velocity field is primarily due to the fact that an effect of magnetic parameter causes an uptick in Lorentz forces involved with the magnetic field, and these magnified Lorentz forces provide further resistance to fluid flow, which causes the velocity field in the boundary layer region to reduce. Figure 2g,h shows the outcome of the porous parameter β on the velocity field for the instances of $S_t = S_0 = 0$ and $S_t = S_0 = 1$, respectively. The velocity field is visibly lowered with higher values of the porosity parameter in the flow zone, as seen in the figures. This drop is
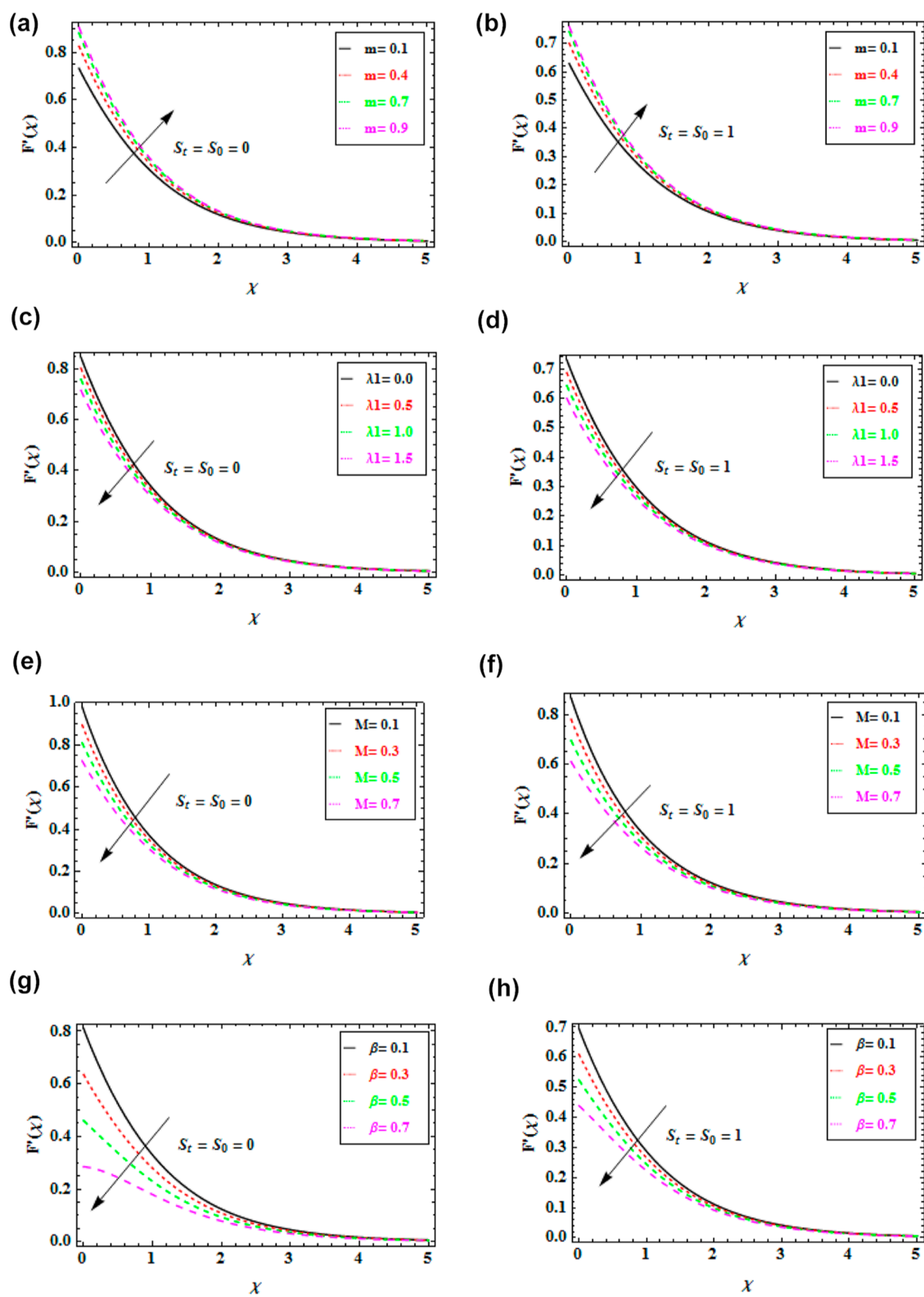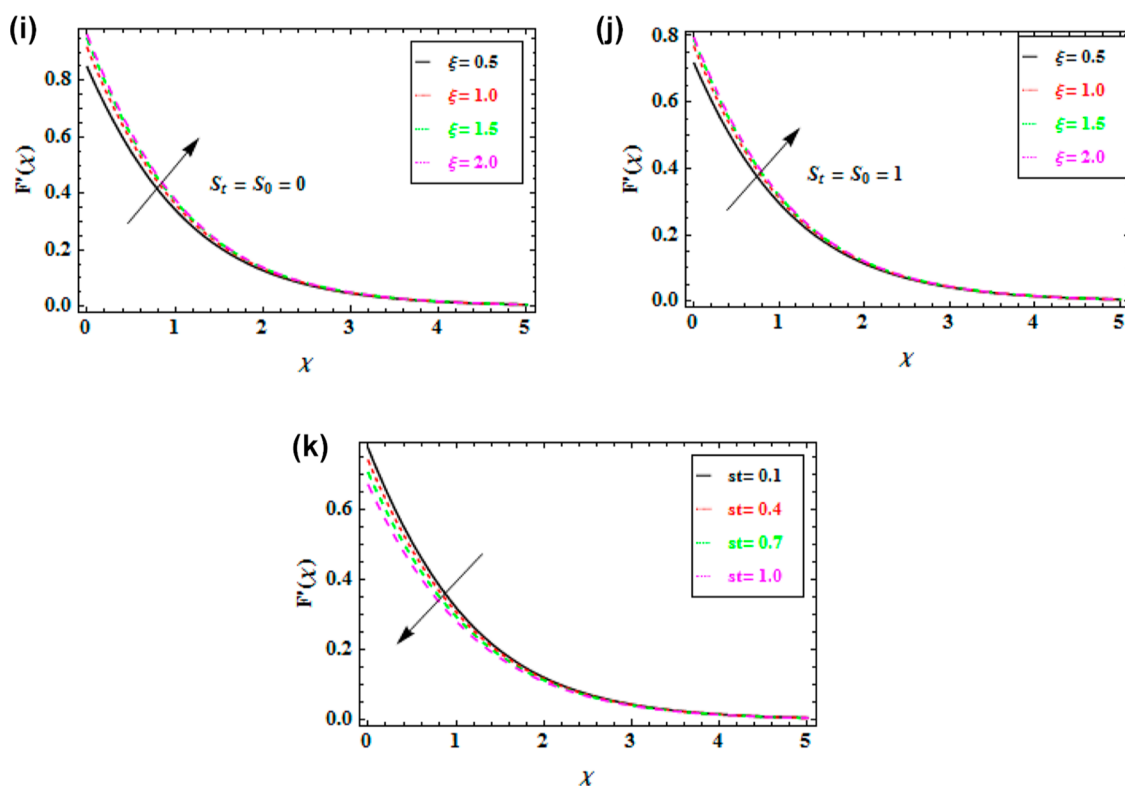
Figure 2. continued

Figure 2. (a) Variation in velocity profile for different values of velocity index m when $S_t = S_0 = 0$. (b) Variation in velocity profile for different values of velocity index m when $S_t = S_0 = 1$. (c) Variation in velocity profile for different fluid parameter λ_1 when $S_t = S_0 = 0$. (d) Variation in velocity profile for different values of fluid parameter λ_1 when $S_t = S_0 = 1$. (e) Variation in velocity profile for different values of magnetic parameter M when $S_t = S_0 = 0$. (f) Variation in velocity profile for different values of magnetic parameter M when $S_t = S_0 = 1$. (g) Variation in velocity profile for different values of porosity parameter β when $S_t = S_0 = 0$. (h) Variation in velocity profile for different values of porosity parameter β when $S_t = S_0 = 1$. (i) Variation in velocity profile for different values of variable viscosity parameter ξ when $S_t = S_0 = 0$. (j) Variation in velocity profile for different values of variable viscosity parameter ξ when $S_t = S_0 = 1$. (k) Variation in velocity profile for different values of thermal stratification parameter S_t.

mostly because of the fact that increasing the values of the porosity parameter causes more and more opposition to fluid flow in the flow zone, which causes the velocity field to decline. The effects of viscosity dependent on the temperature parameter ξ on the velocity profile for the cases $S_t = S_0 = 0$ and $S_t = S_0 = 1$ are shown in Figure 2i,j. A rise in the viscosity parameter results in a significant change in the velocity profile for both cases, as shown in figures. Since the viscosity parameter ξ is inversely related to dimensionless viscosity, as a result, enhancing the viscosity parameter diminishes the dimensionless viscosity and hence lowers the viscous forces that oppose fluid motion. Therefore, inertia forces outnumber viscous forces, and the liquid accelerates. Figure 2k depicts the stimulus of the stratification parameter S_t on the velocity profile. It is noticed that the velocity is enhanced by raising the stratification parameter S_t.

Effects of variation of m on the temperature profile are seen in Figure 3a,b for $S_t = S_0 = 0$ and $S_t = S_0 = 1$,. From both figures, it is clearly seen that the temperature profile declines by enhancing m. Figure 3c,d depicts the temperature profile fluctuations observed for various values of magnetic parameter M. The temperature field is amplified for rising values of M, as can be seen in both diagrams. An increase in M causes the elastic stress variable to drop, resulting in an enlarged temperature field in the region of the flow configuration. Furthermore, because of the existence of the Joule dissipation effect, more heat energy

will be released into the working fluid, causing the temperature profile in the boundary layer region to improve for $S_t = S_0 = 0$ and $S_t = S_0 = 1$. Figure 3e,f portrays temperature field variations for different values of porosity parameter β. Because of an escalation in fluid viscosity or a diminution in the permeability of the porous media near the edge of the boundary layer, the non-dimensional temperature is increased in both cases $S_t = S_0 = 0$ and $S_t = S_0 = 1$. Figure 3g,h shows that the influence of a variable viscosity parameter ξ on the temperature profile for cases $S_t = S_0 = 0$ and $S_t = S_0 = 1$, respectively, and a rise in the value of ξ tends to increase the thickness of the thermal boundary layer. As a result, the values of temperature rise, and the temperature of fluid rises as the ξ rises for unstratified and stratified regions. Figure 3i,j shows the result of the heat generation parameter γ on the temperature profile when $S_t = S_0 = 0$ and $S_t = S_0 = 1$. The temperature profile appears to be increasing as the heat generation parameter is increased. Positive changes in the heat generation parameter γ generate heat in the flow regime, resulting in an increase in fluid temperature for both stratified and unstratified cases. Figure 3k shows the consequence of the thermal stratification parameter S_t on temperature distribution. Positive S_t values indicate a decrease in temperature because higher S_t values indicate a decrease in convective potential between the ambient temperature and paraboloid of revolution.
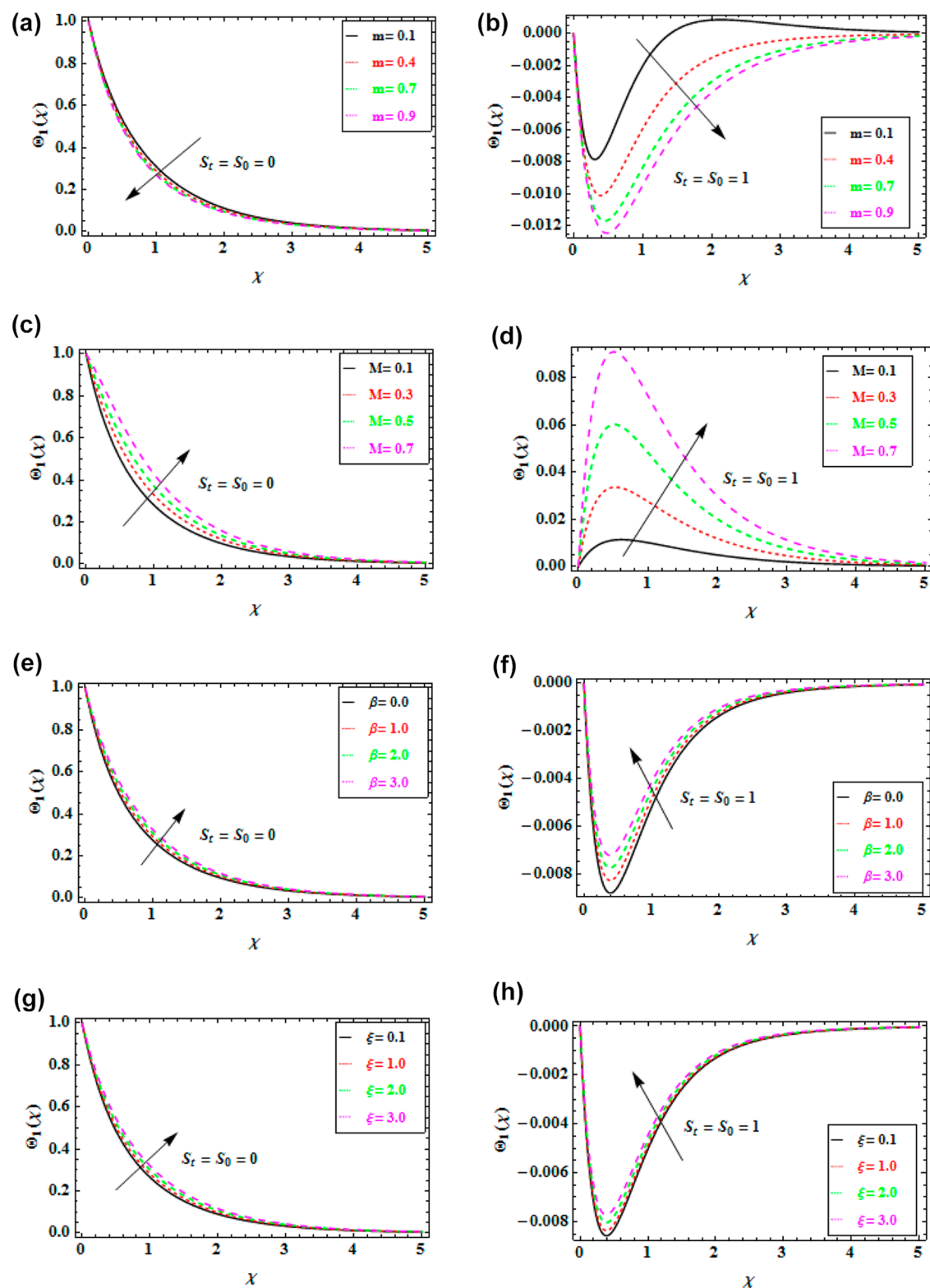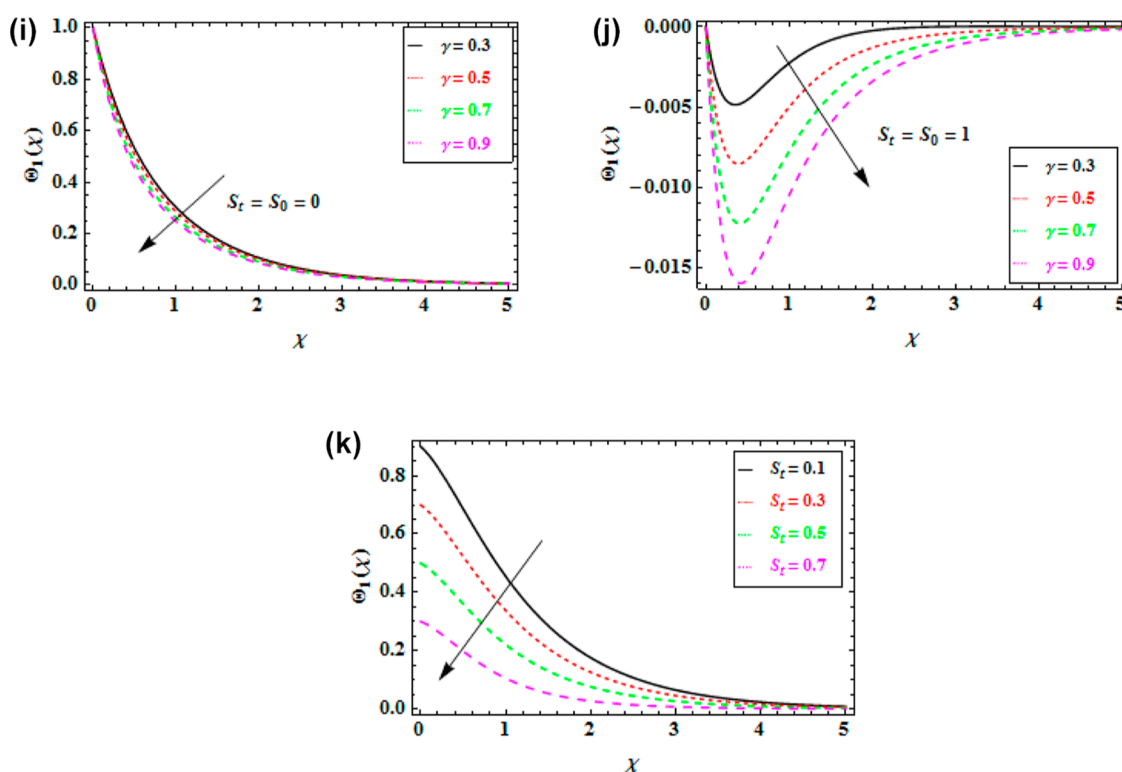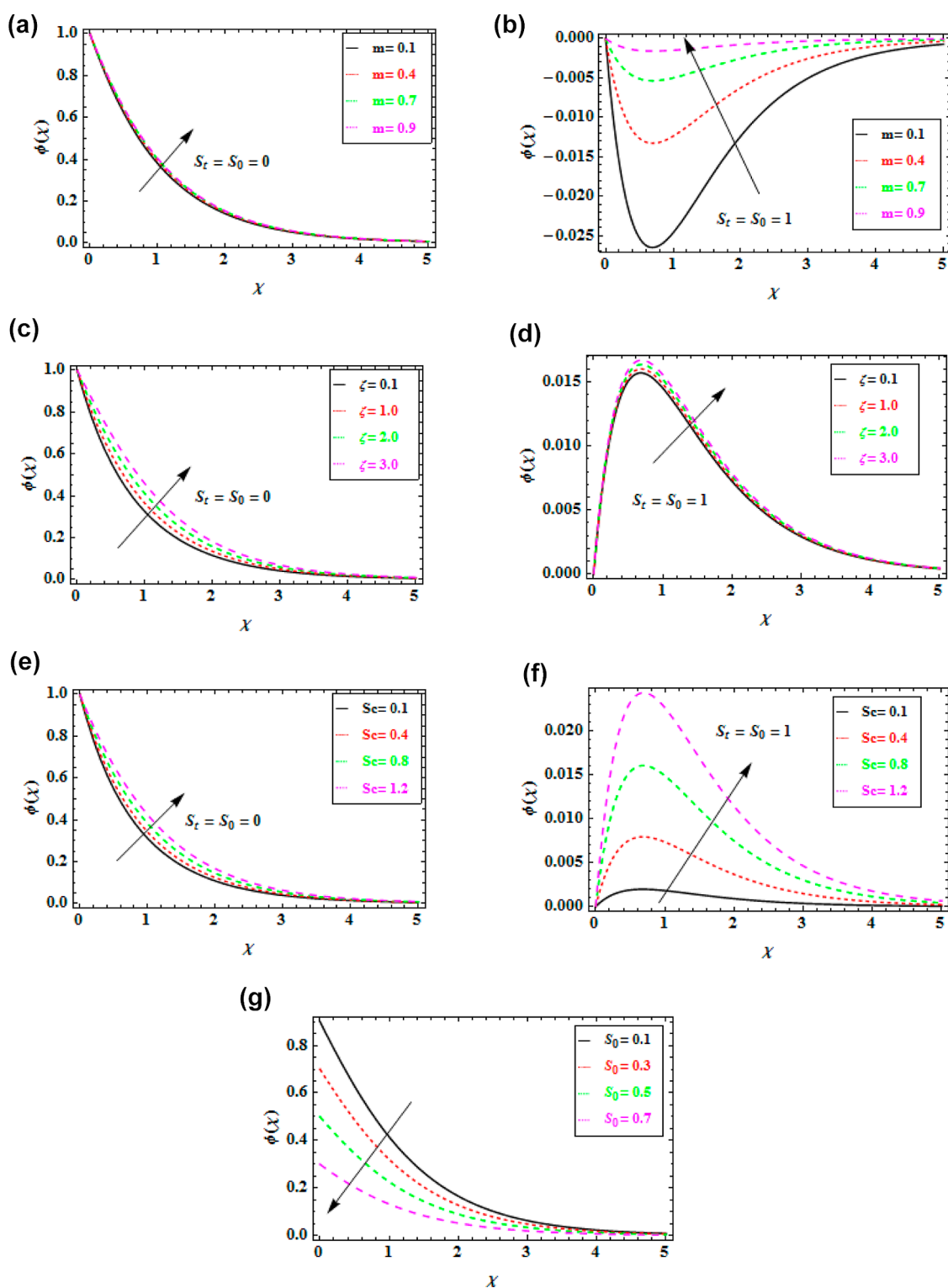
Figure 3. continued

Figure 3. (a) Variation in temperature profile for different values of velocity index m when $S_t = S_0 = 0$. (b) Variation in temperature profile for different values of velocity index m when $S_t = S_0 = 1$. (c) Variation in temperature profile for different values of magnetic parameter M when $S_t = S_0 = 0$. (d) Variation in temperature profile for different values of magnetic parameter M when $S_t = S_0 = 1$. (e) Variation in temperature profile for different values of porosity parameter β when $S_t = S_0 = 0$. (f) Variation in temperature profile for different values of porosity parameter β when $S_t = S_0 = 1$. (g) Variation in temperature profile for different values of variable viscosity parameter ξ when $S_t = S_0 = 0$. (h) Variation in temperature profile for different values of variable viscosity parameter ξ when $S_t = S_0 = 1$. (i) Variation in temperature profile for different values of heat generation parameter γ when $S_t = S_0 = 0$. (j) Variation in temperature profile for different values of heat generation parameter γ when $S_t = S_0 = 1$. (k) Variation in temperature profile for different values of thermal stratification parameter S_t.

The influence of m variation on the concentration fields is shown in Figure 4a,b). When $S_t = S_0 = 0$, the concentration field is observed to be enhanced for larger values of m, whereas when $S_t = S_0 = 1$, the concentration field is observed to be increased from the negative zone for larger values of m. Physically, the observed trend is caused by stratification, which creates a transition zone between the temperature and concentration gradients of cold and hot fluid zones. The effects of the chemical reaction parameter ζ variation on the concentration fields are shown in Figure 4c,d for the unstratified and stratified regions of the paraboloid of revolution. The concentration field is observed to be enhanced for larger values of ζ for both cases. Figure 4e,f depicts the influence of Schmidt number on the concentration profile for cases $S_t = S_0 = 0$ and $S_t = S_0 = 1$. In Figure 4e, a slight increase in the concentration field is observed for Sc variation in an unstratified region of the paraboloid of revolution, whereas in Figure 4f, a significant increase in the concentration field is observed for Sc variation in a stably stratified region of the paraboloid of revolution. Physically, the ratio of momentum diffusivity (viscosity) to mass diffusivity is the Schmidt number, which is a dimensionless quantity. As a result, as the Schmidt number rises, the concentration profile rises as well. The variation in fluid concentration in relation to the solutal stratification parameter S_0 is depicted in Figure 4g. It is observed that the concentration distribution reduces for larger values of the solutal parameter S_0.

This is due to a decrease in the potential difference between surface and ambient concentrations.

The outcome of the Brinkman number on the entropy formation rate for $S_t = S_0 = 0$ and $S_t = S_0 = 1$ is seen in Figure 5a,b. For both the unstratified and stratified cases, the finding demonstrates that the entropy generation rate within the paraboloid of revolution grows as the Brinkman number escalates. The impact of the Brinkman number on the Bejan number is demonstrated in Figure 6a,b for both unstratified and stratified cases, which shows that the Bejan number drops down for a higher Brinkman number. The explanation for this is simple: the Brinkman number is a heat source, and heat is produced inside the layers of moving fluid particles. Entropy formation within the paraboloid of revolution flow is encouraged by the heat created and the heat transmitted from the heat wall. As a result, the Brinkman number must be kept under control in order to decrease entropy. The influences of the magnetic parameter M on entropy production and the Bejan number are shown in Figures 5c, 6c and 5d, 6d for $S_t = S_0 = 0$ and $S_t = S_0 = 1$ cases, respectively. The figures show that as the magnetic parameter M is increased, the extent of local entropy generation increases, while the Bejan number decreases in both unstratified and stratified regions. The magnetic field adds to the fluid's entropy. At the surface, there is also a lot of entropy creation. Figure 5e,f depicts the impact of the temperature ratio parameter Ω on entropy formation for unstratified and stratified cases. From the figures, it is observed that for both unstratified

Figure 4. (a) Variation in concentration profiles for different values of velocity index m when $S_t = S_0 = 0$. (b) Variation in concentration profiles for different values of velocity index m when $S_t = S_0 = 1$. (c) Variation in concentration profiles for different values of chemical reaction parameter ζ when $S_t = S_0 = 0$. (d) Variation in concentration profiles for different values of chemical reaction parameter ζ when $S_t = S_0 = 1$. (e) Variation in concentration profiles for different values of Schmidt number Sc when $S_t = S_0 = 0$. (f) Variation in concentration profiles for different values of Schmidt number Sc when $S_t = S_0 = 1$. (g) Variation in concentration profiles for different values of solute stratification parameter S_0.

and stratified regions, entropy production declines as Ω improves. Figure 6e,f indicates the influence of the temperature ration parameter Ω on the Bejan number for both unstratified and stratified regions. The Bejan number grows up as Ω improves.

Tables 1, 2, and 3 depict the variation of skin friction coefficients, Nusselt number, and Sherwood number for various
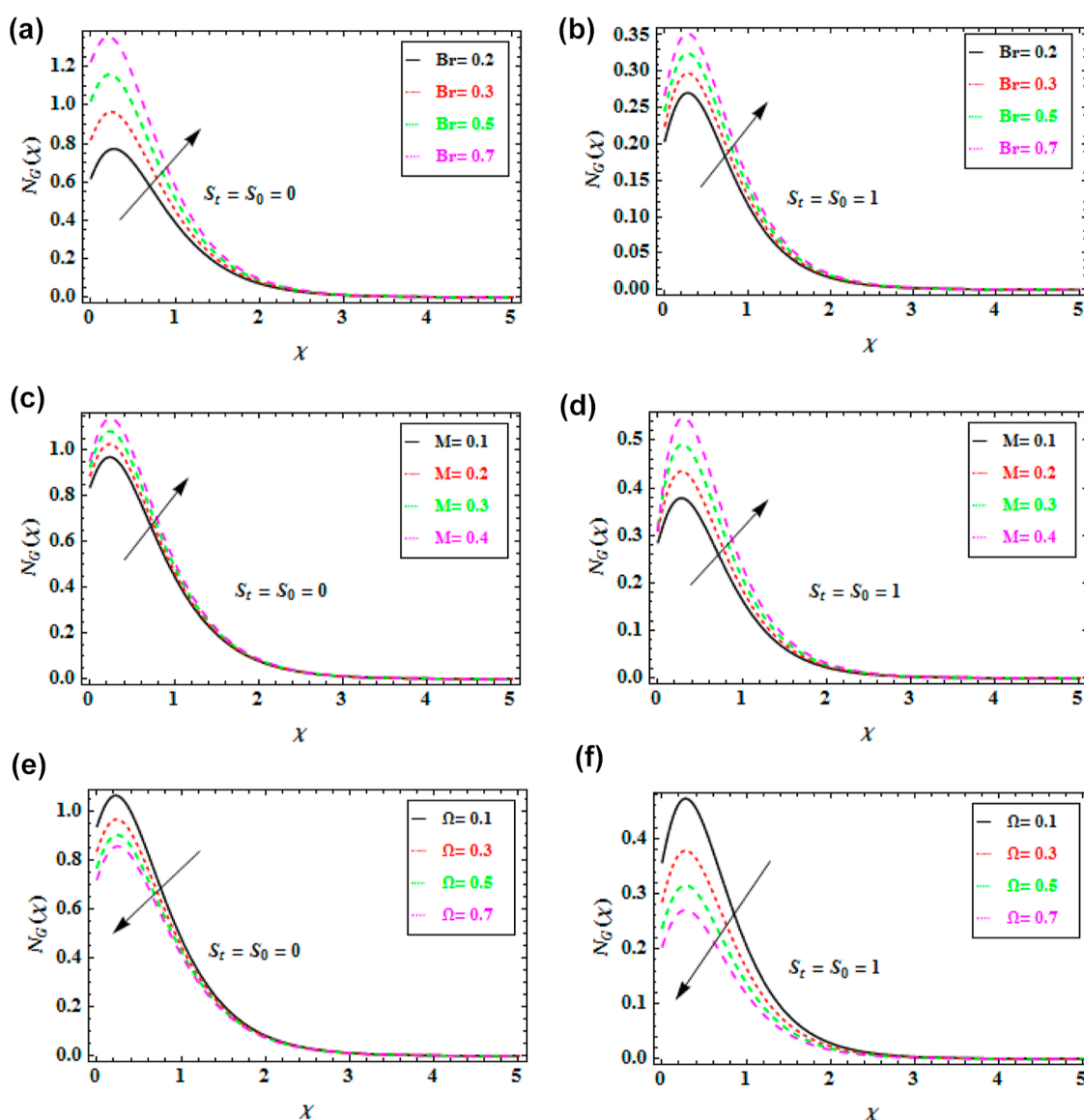
Figure 5. (a) Variation in entropy optimization for different values of Brinkman number Br when $S_t = S_0 = 0$. (b) Variation in entropy optimization for different values of Brinkman number Br when $S_t = S_0 = 1$. (c) Variation in entropy optimization for different values of magnetic parameter M when $S_t = S_0 = 0$. (d) Variation in entropy optimization for diff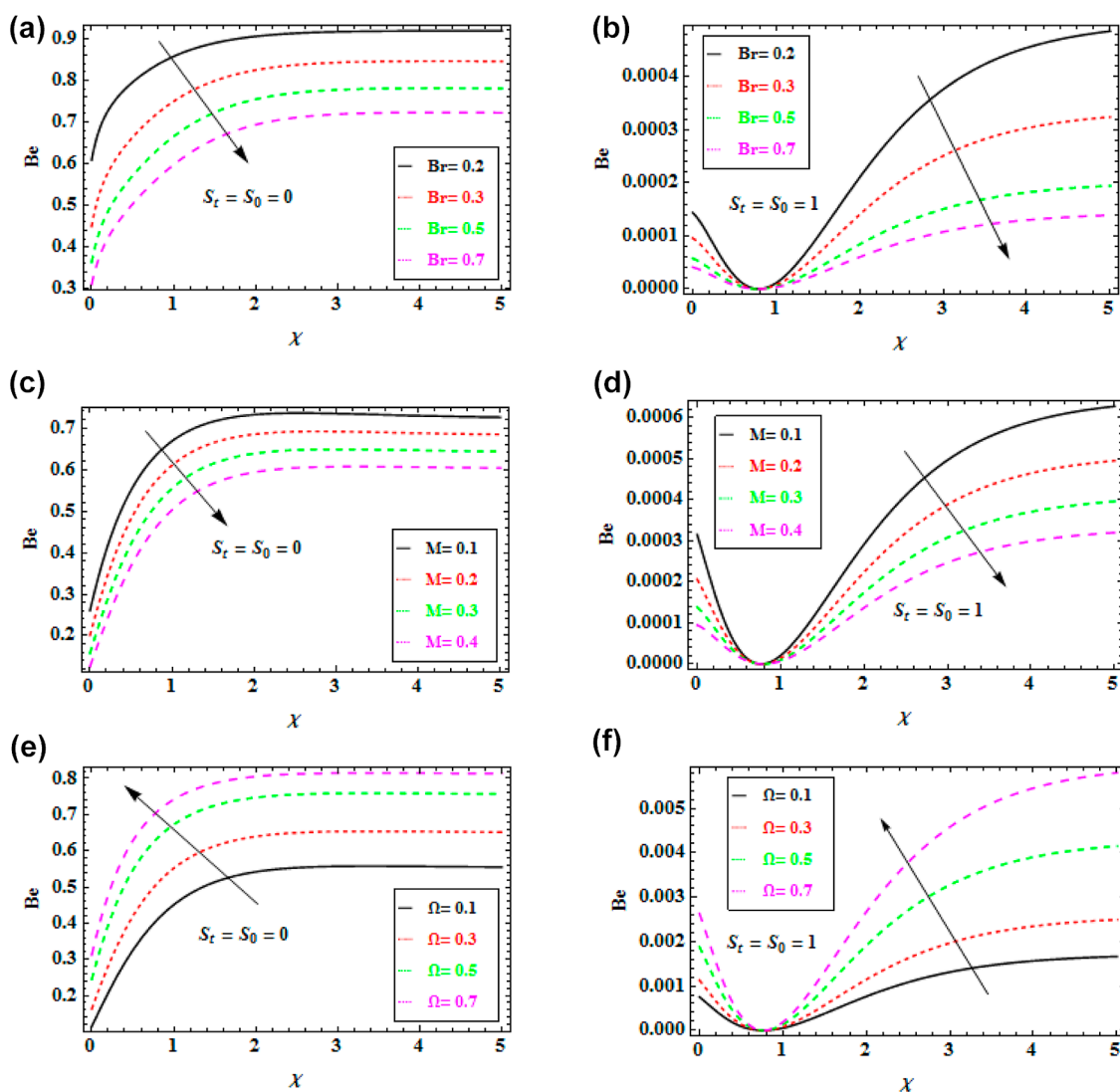erent values of magnetic parameter M when $S_t = S_0 = 1$. (e) Variation in entropy optimization for different values of the temperatureratio parameter Ω when $S_t = S_0 = 0$. (f) Variation in entropy optimization for different values of the temperature−ratio parameter Ω when $S_t = S_0 = 1$.

parameters, respectively. Table 1 indicates the variant of skin friction coefficients for incremental values of the second-grade fluid parameter, magnetic parameter, porosity parameter, and variable viscosity parameter for unstratified and stratified cases. Incremental values of the fluid parameter declined the skin friction coefficient, whereas growing values of the magnetic parameter, porosity parameter, and viscosity parameter upsurge skin friction coefficients for both unstratified and stratified regions. Table 2 indicates the variant of Nusselt number for numerous values of the magnetic parameter, heat generation parameter, radiation parameter, and Eckert number for $S_t = S_0 = 0$ and $S_t = S_0 = 1$. From the table, it is observed that for both unstratified and stratified cases, the Nusselt number upsurges for rising values of M, γ, Rd, and Ec. Tables 3 and 4 indicate the variant of Sherwood number for incremental values of the Schmidt number and chemical reaction parameter for the cases $S_t = S_0 = 0$ and $S_t = S_0 = 1$. The finding demonstrates

that the Sherwood number declined for escalations in the chemical reaction parameter and Schmidt number for both unstratified and stratified regions.

6. CONCLUSIONS

Second-grade fluid flow over a horizontal surface of a paraboloid of revolution has been studied, with emphasis on the unstratified and stably stratified regions. The dimensionless equations have been numerically solved, and the major key outcomes of the study are shortened as follows:

- Velocity profiles increase when the velocity index and variable viscosity parameter upsurge, whereas conflicting behavior is shown for upsurge values of the fluid parameter, magnetic parameter, and porosity parameter for both unstratified and stratified cases.
- Temperature distribution is an increasing function of the magnetic parameter, porosity parameter, and variable

Figure 6. (a) Variation in Bejan number for different values of Brinkman number Br when $S_t = S_0 = 0$. (b) Variation in Bejan number for different values of Brinkman number Br when $S_t = S_0 = 1$. (c) Variation in Bejan number for different values of magnetic parameter M when $S_t = S_0 = 0$. (d) Variation in Bejan number for different values of magnetic parameter M when $S_t = S_0 = 1$. (e) Variation in Bejan number for different values of temperature ratio parameter Ω when $S_t = S_0 = 0$. (f) Variation in Bejan number for different values of the temperature ratio parameter Ω when $S_t = S_0 = 0$.

Table 1. Variation of Skin Friction for Numerous Parameters

λ_1	M	β	ξ	$Re_x^{1/2}C_f$ $S_t = S_0 = 0$	$Re_x^{1/2}C_f$ $S_t = S_0 = 1$
0.0				−0.79999	−0.74799
0.5				−1.54439	−1.40753
1.0				−2.22858	−2.01121
	0.1			−2.032141	−1.88437
	0.3			−1.86643	−1.72229
	0.5			−1.70385	−1.56335
		0.1		−1.84897	−1.64243
		0.3		−1.561946	−1.48505
		0.5		−1.28781	−1.33079
			0.1	−1.72802	−1.58771
			0.3	−1.67888	−1.53819
			0.5	−1.62656	−1.48549

Table 2. Variation of the Nusselt Number for Various Parameters

M	γ	Rd	Ec	$Re_x^{-1/2}N_u$ $S_t = S_0 = 0$	$Re_x^{-1/2}N_u$ $S_t = S_0 = 1$
0.1				1.366413	−0.173012
0.3				1.381303	−0.1509507
0.5				1.394915	−0.1302655
	0.1			1.966641	−0.17356005
	0.3			2.111575	−0.020312
	0.5			2.256512	0.132937
		0.1		1.013456	−0.0995668
		0.3		1.263412	−0.1198638
		0.5		1.530895	−0.140836
			0.1	1.373282	−0.1521856
			0.3	1.416549	−0.1083453
			0.5	1.459818	−0.0645039

Table 3. Variation of the Sherwood Number for Different Parameters

Sc	Z	$Re_x^{-1/2}S_h$ $S_t = S_0 = 0$	$Re_x^{-1/2}S_h$ $S_t = S_0 = 1$
0.1		1.1295706	−0.0045168
0.3		1.1042614	−0.01355805
0.5		1.0789438	−0.0226091
	0.1	1.1212254	−0.0135447
	0.3	1.1099196	−0.0135536
	0.5	1.0985996	−0.0135625

Table 4. Comparison of the Obtained Result of $f''(0)$ With That of Kalyani et al[10]

m_1	present paper	Kalyani et al.[10]
0.1	−0.86727272	−0.86710093
0.2	−0.85333334	−0.8624051
0.3	−0.84153846	−0.8584863
0.4	−0.83142857	−0.8481544

viscosity parameter, whereas it is a declining function of velocity index and heat generation parameter for both unstratified and stratified cases.

- For unstratified and stratified cases, there is enhancement in the concentration profile for large values of the velocity index parameter, chemical reaction parameter, and Schmidt number.
- Velocity and temperature profiles declined for large values of the thermal stratification parameter.
- For large values of the solute stratification parameter, concentration profiles fall down.
- For both unstratified and stratified regions, incremental values of the Brinkman number and magnetic parameter depict augmentation in the entropy production, while entropy production drops for a large value of the temperature ratio parameter.
- Skin friction coefficients rise up for incremental values of the magnetic parameter, porosity parameter, and variable viscosity parameter while decline for incremental values of the fluid parameter for both unstratified and stratified regions.
- The Nusselt number declined for growing values of the magnetic parameter, heat generation parameter, radiation parameter, and Eckert parameter for both unstratified and stratified regions.
- For large values of the chemical reaction parameter and Schmidt number, the Sherwood number for unstratified and stratified cases declined.

■ AUTHOR INFORMATION

Corresponding Authors

Narcisa Vrinceanu − *Faculty of Engineering, Department of Industrial Machines and Equipments, "Lucian Blaga" University of Sibiu, Sibiu 5500204, Romania;* Email: vrinceanu.narcisai@ulbsibiu.ro

Zahir Shah − *Department of Mathematical Sciences, University of Lakki Marwat, Lakki Marwat 28420 Khyber Pakhtunkhwa, Pakistan;* ⓞ orcid.org/0000-0002-5539-4225; Email: Zahir@ulm.edu.pk

Authors

Meshal Shutaywi − *Department of Mathematics, College of Science and Arts, King Abdul-Aziz University, Rabigh 21911, Saudi Arabia*

Muhammad Rooman − *Department of Mathematical Sciences, University of Lakki Marwat, Lakki Marwat 28420 Khyber Pakhtunkhwa, Pakistan*

Muhammad Asif Jan − *Department of Mathematics, Kohat University of Science and Technology KUST, Kohat 26000 Khyber pakhtoonkhwa, Pakistan*

Wejdan Deebani − *Department of Mathematics, College of Science and Arts, King Abdul-Aziz University, Rabigh 21911, Saudi Arabia*

Complete contact information is available at:
https://pubs.acs.org/10.1021/acsomega.2c02452

■ NOMENCLATURE

A, b	Arbitrary constant
B_0	magnetic field strength
Br	Brinkman number
c_p	specific heat transfer (J kg^{-1} K^{-1})
C	concentration
D	Brownian motion
Ec	Eckert number
k	thermal conductivity (W m^{-1} K^{-1})
k_1	permeability of porous medium
k^*	absorption coefficient
K^*	chemical reaction
M	magnetization (A m^{-1})
m	velocity index
n	intensity of internal heat generation
Pr	Prandtl number
Q_0	heat generation/absorption
Rd	thermal radiation
Sc	Schmidt number
S_t	thermal stratification
S_0	solute stratification
T	temperature of fluid
u, v	velocity components (m s^{-1})
U_0	reference velocity
x, y	coordinate axis (m)

■ GREEK LETTER

α_1	material parameter
β	porosity parameter
γ	space-dependent internal heat source parameter
ξ	temperature-dependent viscous parameter
ζ	chemical reaction parameter
F	surface thickness
η	independent coordinate
λ_1	second-grade fluid parameter
μ	dynamic viscosity
μ_0	magnetic permeability
ϑ	kinematic viscosity

ρ   density (kg m^{-3})
ρC_p heat capacitance
σ   electrical conductivity
σ*   Stefan−Boltzmann constant
ψ   stream function (m^2 s^{-1})

■ REFERENCES

(1) Vajravelu, K.; Roper, T. Flow and heat transfer in a second grade fluid over a stretching sheet. *Int. J. Non Lin. Mech.* 1999, 34, 1031−1036.

(2) Rajeswari, G. K.; Rathna, S. L. Flow of a particular class of non-Newtonian visco-elastic and visco-inelastic fluids near a stagnation point. *undefined* 1962, 13, 43−57.

(3) Garg, V. K.; Rajagopal, K. R. Flow of a non-Newtonian fluid past a wedge. *undefined* 1991, 88, 113−123.

(4) Fetecau, C.; Fetecau, C. Starting solutions for the motion of a second grade fluid due to longitudinal and torsional oscillations of a circular cylinder. *undefined* 2006, 44, 788−796.

(5) Abbas, N.; Malik, M. Y.; Nadeem, S.; Hussain, S.; El-Shafa, A. S. Similarity solution of second grade fluid flow over a moving cylinder. *Int. J. Mod. Phys. B* 2021, 35, 2150325.

(6) Davis, R. T.; Werle, M. J. Numerical solutions for laminar incompressible flow past a paraboloid of revolution. *AIAA J.* 1972, 10, 1224−1230.

(7) Makinde, O. D.; Animasaun, I. L. Thermophoresis and Brownian motion effects on MHD bioconvection of nanofluid with nonlinear thermal radiation and quartic chemical reaction past an upper horizontal surface of a paraboloid of revolution. *J. Mol. Liq.* 2016, 221, 733−743.

(8) Zeeshan, A.; Awais, M.; Alzahrani, F.; Shehzad, N. Energy analysis of non-Newtonian nanofluid flow over parabola of revolution on the horizontal surface with catalytic chemical reaction. *Heat Transf* 2021, 50, 6189−6209.

(9) Abdeljawad, T.; Ullah, A.; Alrabaiah, H.; Ikramullah, M.; Ayaz, M.; Khan, W.; Khan, I.; Khan, H. U. Thermal Radiations and Mass Transfer Analysis of the Three-Dimensional Magnetite Carreau Fluid Flow Past a Horizontal Surface of Paraboloid of Revolution. *Process* 2020, 8, 656.

(10) Kalyani, K.; Namana, S. R.; Sudha Rani, M. V. V. N. L. A numerical study on cross diffusion cattaneo-christov impacts of MHD micropolar fluid across a paraboloid. *Iraqi J. Sci.* 2021, 62, 1238−1264.

(11) Khan, M.; Rasheed, A.; Salahuddin, T.; Ali, S. Chemically reactive flow of hyperbolic tangent fluid flow having thermal radiation and double stratification embedded in porous medium. *Ain Shams Eng. J.* 2021, 12, 3209−3216.

(12) Dawar, A.; Saeed, A.; Islam, S.; Shah, Z.; Kumam, W.; Kumam, P. Electromagnetohydrodynamic bioconvective flow of binary fluid containing nanoparticles and gyrotactic microorganisms through a stratified stretching sheet. *Sci. Rep.* 2021, 11, 23159.

(13) Khan, W. A.; Anjum, N.; Waqas, M.; Abbas, S. Z.; Irfan, M.; Muhammad, T. Impact of stratification phenomena on a nonlinear radiative flow of sutterby nanofluid. *J. Mater. Res. Technol.* 2021, 15, 306−314.

(14) Luo, T.; Wang, J. Effects of Atwood number and stratification parameter on compressible multi-mode Rayleigh−Taylor instability. *Phys. Fluids* 2021, 33, 115111.

(15) Kolade Koriko, O.; Oreyeni, T.; John Omowaye, A.; Lare Animasaun, I. Homotopy Analysis of MHD Free Convective Micropolar Fluid Flow along a Vertical Surface Embedded in Non-Darcian Thermally-Stratified Medium. *Open J. Fluid Dynam.* 2016, 06, 198−221.

(16) Pattnaik, P. K.; Bhatti, M. M.; Mishra, S. R.; Abbas, M. A.; Bég, O. A. Mixed Convective-Radiative Dissipative Magnetized Micropolar Nanofluid Flow over a Stretching Surface in Porous Media with Double Stratification and Chemical Reaction Effects: ADM-Padé Computation. *J. Math.* 2022, 2022, 1−19.

(17) Bejan, A. A Study of Entropy Generation in Fundamental Convective Heat Transfer. *J. Heat Transfer* 1979, 101, 718−725.

(18) Shit, G. C.; Haldar, R.; Mandal, S. Entropy generation on MHD flow and convective heat transfer in a porous medium of exponentially stretching surface saturated by nanofluids. *Adv. Powder Technol.* 2017, 28, 1519−1530.

(19) Shit, G. C.; Mandal, S. Entropy Analysis on Unsteady MHD Flow of Casson Nanofluid over a Stretching Vertical Plate with Thermal Radiation Effect. *Int. J. Comput. Appl. Math.* 2020, 6, 2.

(20) Bhatti, M. M.; Sheikholeslami, M.; Shahid, A.; Hassan, M.; Abbas, T. Entropy generation on the interaction of nanoparticles over a stretched surface with thermal radiation. *Colloids Surf., A* 2019, 570, 368−376.

(21) Kumar, A.; Tripathi, R.; Singh, R. Entropy generation and regression analysis on stagnation point flow of Casson nanofluid with Arrhenius activation energy. *J. Braz. Soc. Mech. Sci. Eng.* 2019, 41, 306.

(22) Bhatti, M. M.; Öztop, H. F.; Ellahi, R.; Sarris, I. E.; Doranehgard, M. H. Insight into the investigation of diamond (C) and Silica (SiO2) nanoparticles suspended in water-based hybrid nanofluid with application in solar collector. *J. Mol. Liq.* 2022, 357, 119134.

(23) Bhatti, M. M.; Bég, O. A.; Abdelsalam, S. I. Computational Framework of Magnetized MgO-Ni/Water-Based Stagnation Nano-flow Past an Elastic Stretching Surface: Application in Solar Energy Coatings. *Nanomaterials* 2022, 12, 1049.

(24) Zhang, L.; Bhatti, M. M.; Michaelides, E. E.; Marin, M.; Ellahi, R. Hybrid nanofluid flow towards an elastic surface with tantalum and nickel nanoparticles, under the influence of an induced magnetic field. *Eur. Phys. J. Spec. Top.* 2022, 231, 521−533.

(25) Kristiawan, B.; Rifa'i, A. I.; Enoki, K.; Wijayanta, A. T.; Miyazaki, T. Enhancing the thermal performance of TiO2/water nanofluids flowing in a helical microfin tube. *Powder Technol.* 2020, 376, 254−262.

(26) Kimura, S.; Bejan, A. The "Heatline" Visualization of Convective Heat Transfer. *J. Heat Transfer* 1983, 105, 916−919.

(27) Purnama, B.; Rahmawati, R.; Wijayanta, A. T.; Suharyana, S. Dependence of Structural and Magnetic Properties on Annealing Times in Co-precipitated Cobalt Ferrite Nanoparticles. *J. Magn. Reson.* 2015, 20, 207−210.

(28) Pranowo; Makarim, D. A.; Suami, A.; Wijayanta, A. T.; Kobayashi, N.; Itaya, Y. Marangoni convection within thermosolute and absorptive aqueous LiBr solution. *Int. J. Heat Mass Tran.* 2022, 188, 122621.

(29) Pranowo; Wijayanta, A. T. Numerical solution strategy for natural convection problems in a triangular cavity using a direct meshless local Petrov-Galerkin method combined with an implicit artificial-compressibility model. *Eng. Anal. Bound. Elem.* 2021, 126, 13−29.

(30) Charraudeau, J. Influence de gradients de proprietes physiques en convection forcee—Application au cas du tube. *Int. J. Heat Mass Tran.* 1975, 18, 87−95.

(31) Batchelor, G. K. *An Introduction to Fluid Dynamics*; Cambridge University Press: London, 1987.